

The enabling electronic motif for topological insulation in ABO_3 perovskites and its structural stability

Xiuwen Zhang^{1,2,*}, Leonardo B. Abdalla¹, Qihang Liu^{1,*}, and Alex Zunger^{1,*}

¹Renewable and Sustainable Energy Institute, University of Colorado, Boulder, Colorado 80309, USA

²College of Electronic Science and Technology, Shenzhen University, Shenzhen, Guangdong, P. R. China

*Email: xiuwen.zhang@colorado.edu; qihang.liu@colorado.edu; alex.zunger@colorado.edu

Keywords: topological insulators; oxide perovskites; structural stability; density functional theory

Abstract

Stable oxide topological insulators (TI's) that could bring together the traditional oxide functionalities with the dissipationless surface states of TI's have been sought for years but none was found. Yet, heavier chalcogenides (selenides, tellurides) were readily found to be TI's. We clarify here the basic contradiction between TI-ness and stability which is maximal for oxides, and trace the basic design principles necessary to identify the window of opportunity of stable TI's. We first identify the electronic motif that can achieve topological band inversion ('topological gene') in ABO_3 as being a lone-pair electron-rich B atom (e.g. Te, I, Bi) at the octahedral site. We then illustrate that poorly screened oxide systems with large inversion energies can undergo energy-lowering atomic distortions that remove the band inversion. We identify the coexistence windows of TI functionality and structure stability for different pressures and find that the common cubic ABO_3 structures have inversion energies lying outside this coexistence window at zero pressure but could be moved into the coexistence window at moderate pressures. Our study demonstrates the interplay between topological band inversion and structural stability and traces the principles needed to design stable oxide topological insulators at ambient pressures.

1. Introduction

Topological insulators (TI's) are materials having an inverted order of the occupied valence and unoccupied conduction bands at time-reversal invariant (TRI) wave vectors in the Brillouin zone (BZ), and can be characterized by the topological invariant^[1] $Z_2 = 1$. Theory then assures that in lower-dimensional forms (2D surface or 1D edge) of the topological bulk system there will be states that possess passivation-resistant, linearly dispersed and mutually crossing (metallic) energy bands^[2]. The required band inversion in the parent bulk system is generally achieved by introducing high atomic number (Z) cations and anions having strong spin-orbit coupling (SOC)^[3-8]. However, such heavy-atom compounds tend to pose defective crystal structures (e.g., spontaneous vacancy formation causing metallic, not insulating behavior) associated with the relatively low cohesion of the weak heavy-atom chemical bonds^[9-11]. The recent quest of topological insulators in oxides^[12-18] has been partially motivated by the hope that this will deliver defect-tolerant lattices, often characteristic of metal oxides^[19], while at the same time affording the integration of topological properties with the rich oxide functionalities such as transparent conductivity^[20], ferroelectricity^[21], ferromagnetism^[22], or superconductivity^[23]. However, the electronic structures of common octet metal oxides, such as ABO_3 perovskites or A_2BO_4 spinels, show that while they may be stable and have wide energy band gaps^[19] E_g , they generally lack band inversion, having a trivial topological invariant $Z_2 = 0$. For example, the common ABO_3 perovskite have oxygen-derived valence bands and B-atom-derived conduction bands [see **Figure 1(a,b)**], hence no band inversion. Indeed, whereas numerous topological insulators have been experimentally observed in selenides and tellurides (e.g. Bi_2Se_3 ^[4] and Bi_2Te_3 ^[24]), stable oxide TI's are yet unknown. Anecdotal examples (discussed in Supplementary Section I) abound of theoretically proposed wide gap oxide TI's in *assumed hypothetical* crystal structures that turned out, however, to be significantly unstable when

energy-lowering structural relaxation were explored in such hypothetical structures^[12-18, 25-30],

We conjecture that the conditions needed for TI-ness—depopulation of bonding valence band states and the occupation of anti-bonding conduction band states—may be contraindicated to thermodynamic stability, if carried out throughout a significant portion of the Brillouin zone. If left unscreened (as in strongly ionic systems), such destabilizing forces may drive structural deformations that alter the crystal symmetry and could undo the band inversion, as illustrated below. Although metastable structures can certainly be made^[31-33], it would be desirable to predict compounds that are TI in not-too-unstable structures, which can be synthesized without fear of producing a topologically trivial but stabler structure, or decomposing after synthesis to a combination of phases that may not be TI's. In this work we report the results of *ab-initio* co-evaluation of TI-ness and stability for a class of oxides perovskites, elucidating the physical origin of the hitherto mysterious difficulty to obtain simultaneously the *electronic* features leading to TI-ness ('topological gene') and the *structural* features of the corresponding lattice structure in ABO₃ oxides. We identify the topological gene that can achieve topological band inversion in oxide perovskites as being a lone-pair electron-rich B atom (e.g., Te, I, Bi) rather than Ti, Nb, Y, respectively) at the octahedral site in the cubic ABO₃. Oxides tend to have larger predicted inversion energies ($\Delta_i > 1$ eV) than selenides or tellurides ($\Delta_i < 0.4$ eV^[4, 24]), and are generally less covalent than the heavier chalcogenides where lattice distortions would be partially screened by the more delocalized electronic states. We then illustrate that poorly screened oxide systems with large inversion energies can undergo energy-lowering atomic distortions that remove the topological band inversion. Favorable screening exists in oxides at higher pressures, and lead to stable oxide TI's as illustrated here for BaTeO₃ and RbIO₃

under moderate pressures. *Covalent oxides* with strong metal-oxygen orbital mixing^[34] do exist and point to the direction of future search for stable oxide TI's at ambient pressures.

2. Topological gene and stability gene

To address this issue we introduce two constructs: We first identify an *electronic* motif within a group of ABO_3 oxides that would generate band inversion—the “*topological gene*” of this group of compounds. As Fig. 1(c, d) illustrates the “topological gene” here is the octahedral BO_6 motif with *lone pair B atom* (generated, e.g., by replacing an electron-poor Ti atom in $BaTiO_3$ by an electron-rich Te atom in $BaTeO_3$ that has an additional $d^{10}s^2$ shell). Second, we examine the stability of the crystal structure that hosts the topological gene, relative to the ground state structures that hosts the “*stability gene*” of this group of compounds. The key challenge is to see if structures with the topological gene can also have the stability gene. Thus, *co-evaluation* of the electronic structure and stability is required.

We confirm via calculated band structures in the framework of density function theory (DFT) using projector-augmented wave (PAW) pseudopotential with the exchange-correlation of Perdew-Burke-Ernzerhof (PBE)^[35-37], and the calculated topological invariant^[38, 39] Z_2 (see Methods Section and Supplementary Section II for the details of calculation methods) that twelve ABO_3 compounds ($BaTeO_3$, $SrTeO_3$, $CaTeO_3$, $BaSeO_3$, $SrSeO_3$, $CaSeO_3$, $RbIO_3$, KIO_3 , $NaIO_3$, $RbBrO_3$, $KBrO_3$, $NaBrO_3$) in the *assumed* cubic perovskite structure with lone-pair B atoms at the octahedral site are in fact TI's, whereas the corresponding compounds with non-lone-pair B ions at the octahedral site (e.g., $BaTiO_3$ and $KNbO_3$) are found to be normal insulators. This substantiates the identity of the topological gene in ABO_3 compounds. However, the crystal structure that host this topological gene is not the stablest structure at this composition: total energy relaxation calculations reveal that the cubic topological structures would relax to lower energy non-cubic perovskite

phases that are not TI's. This is consistent with the above-mentioned topology vs stability conjecture. Indeed, by performing constrained DFT calculations (see Methods Section), we observe a regained stability of the cubic phase. We further identified the window of coexistence of TI-ness and stability at ambient conditions, and find that the topological cubic ABO_3 phases have inversion energies lying outside this coexistence window. Building upon this identification, we find that moderate external pressure can significantly expand the above coexistence window, and eventually leads to simultaneously stable and topological cubic ABO_3 phases, thus bringing the 'stability gene' into coincidence with the 'topological gene'. This study illustrates the interplay between the topological gene needed to obtain band inversion and the structural motif needed for stability in the ABO_3 oxides, and traces the window of opportunity to design stable oxide TI's at ambient pressures.

3. Electronic requirements for the topological gene in cubic ABO_3 perovskites

In conventional ABO_3 compounds with electron-poor B atoms [such as illustrated in Fig. 1(b)] the occupied valence band is oxygen derived whereas the empty conduction states are B-atom derived with normal, *s*-below-*p* orbital order (thus, no inversion). To induce band inversion, one would like to change the order of B atom orbitals to *p*-below-*s* and assure that the Fermi energy is located between these occupied and unoccupied states, respectively. The idea is to replace the B atom in ABO_3 in the cubic perovskite structure [see the inset of Fig. 1(c)] by an electron-rich B element of the same formal charge. Such a B atom has an occupied (lone pair) *s* orbital below its empty *p* orbital, yet above the O-*p* state, as shown in Fig. 1(c). The lone pair *s* orbital can thus become an unoccupied state above the conduction band due to (B-atom *s*)-(oxygen *p*) level repulsion, leading to band inversion (B-*p* below B-*s*) as well as to a finite excitation band gap between B-*p* (occupied) and B-*s* (unoccupied), which is illustrated in Fig. 1(d). We will illustrate via quantitative DFT

calculations the above concept and its rather broad applicability for different groups of perovskite compounds.

In the $\text{II}_A\text{-IV}_A\text{-O}_3$ group of compounds exemplified by BaTiO_3 , we replace Ti^{4+} by the electron-richer Te^{4+} having additional $d^{10}s^2$ shell, leading to the $\text{II}_A\text{-VI}_B\text{-O}_3$ group of compounds exemplified by BaTeO_3 . Two effects, noted by our detailed DFT calculations and illustrated by a simple orbital diagram [see Fig. 1] are associated with this transmutation: (i) Because of the addition of $d^{10}s^2$ shell (where the s^2 lone-pair band is occupied), the outmost B- d and B- s states of B = Te become occupied, with a band gap located between B- s and B- p states [see Fig. 1(c,d)]. The outer s , p , and d atomic orbitals of B = Te drop in energy relative to B = Ti (because of the less screening of the core by the valence shell). (ii) The relativistic Darwin^[40] effect causes the s orbital to become relatively localized and introduce an *occupied* lone-pair s -band, which in this case lies above the O- p bands. Since in the cubic perovskite structure Te (in BaTeO_3) or Ti (in BaTiO_3) are located at the octahedral O_h site where they are bonded to six O atoms, there will be a level repulsion between the O- p and Te- s bands, displacing the Te- s band upwards. If the repulsion is strong enough, as it is at the R point in the BZ [see Fig. 1(e)], this repulsion will place Te- s above Te- p [see Fig. 1(d)], leading to band inversion between Te- s and Te- p states at R point in the Pm-3m structure [see **Figure 2(a)**]. *Therefore, the use at the B site of the electron-rich version (Te in place of Ti) causes band inversion, thus constituting the topological gene in these systems.*

Fig. 1(a,e) illustrates this design principle via DFT band structure. We see that while in BaTiO_3 the conduction band minimum (CBM) is composed of Ti-atom 3d states (yellow) throughout BZ, in BaTeO_3 there is a band inversion at R point where the valence band maximum (VBM) is made of Te- p orbital (green) instead of Te- s orbital (red). Calculation of the topological invariant from the wavefunctions (see Methods Section) finds $Z_2 = 1$ in

BaTeO₃ as compared to the expected $Z_2 = 0$ in BaTiO₃. That this design principle is rather general can be seen by considering other leading ABO₃ perovskite prototypes.

In the **I_A-V_A-O₃** group of compounds exemplified by KNbO₃, we replace Nb⁵⁺ by I⁵⁺ leading to the group **I_A-VII_B-O₃** exemplified by KIO₃. Supplementary Section III compares the electronic structures of KNbO₃ and KIO₃. We find $Z_2 = 0$ in KNbO₃ whereas $Z_2 = 1$ in KIO₃ [41]. The Supplementary Section IV provides the values of the excitation gaps in the compounds designed according to the topological gene, and discusses effects due to possible DFT errors as compared to Hybrid functional (HSE06 [42]) calculations. The results show that the inversion energy (Δ_i), i.e., the gap between the inverted valence and conduction bands at TRI wave vectors, is slightly reduced (by 4%) in HSE06 as compared to DFT, indicating that the band inversion discussed here is quite robust against DFT errors.

4. Band inversion is often contraindicated to stability

Having identified and verified an *electronic* motif—the topological gene—we next ask whether the crystal structure (here, cubic ABO₃ perovskite) that harbors the topology coincides with the structure that harbors stability.

Figure 3 shows the total energies (in meV/atom, given in parentheses) of various ABO₃ structures (denoted S1-S15 in Fig. 2, S1 being the cubic perovskite structure while S2-S15 being the lowest-energy structures of specific ABO₃ compounds), relative to the lowest-energy phase. In addition to stability, Fig. 3 also denotes if according to the calculated topological invariant Z_2 the compound is a TI or a normal insulator (NI). *We find from such total energy minimizations that the BO₆ octahedral unit with the said electron rich B atom tends to distort towards a stabler, non-cubic crystal structures [29, 30] and that this distortion removes the band inversion and thus TI-ness.* Therefore, the stability gene and TI gene tend to contradict each other for the ABO₃ compounds at ambient conditions.

To get a deeper understanding on the interplay between structural stability and band inversion, we perform constrained DFT calculations constructed for tuning band inversion to examine its effect on the total energy. The tuning of the inversion energy can be done by using an external potential that shifts upwards the B atom p orbital energy, thus, according to Fig. 1(d) the inverted structure (p -below- s) can be tuned to be un-inverted (s -below- p). This constraint can be implemented, for example, by adding an external potential term^[43] V_p to the DFT Hamiltonian acting on the I - p orbital in RbIO_3 . We then monitor the total energy of the cubic perovskite structure (S1) relative to its stable R3m rhombohedral phase [S2, see Fig. 2(b)], as a function of Δ_i . **Figure 4(a)** shows that as Δ_i decreases, the energy of the cubic S1 phase (relative to S2) also decreases, indicating that band inversion is contraindicated with the stability of crystal structure (see Supplementary Section V for the evolution of the electronic structures with decreasing inversion energy). *Significantly, however, there is a narrow window ($0 < \Delta_i < 0.8$ eV) shown by red background in Fig. 4(a), where topological band inversion and the stability of the band-inverted crystal structure can coexist.* It is noticed that the currently known stable TI's (e.g. Bi_2Se_3 ^[4] and Bi_2Te_3 ^[24]) have Δ_i much smaller than 0.8 eV, lying inside the coexistence window ($0 < \Delta_i < 0.8$ eV). Whereas the cubic ABO_3 structures with short B-O bonds have $\Delta_i > 1$ eV due to the strong coupling between B- s and O- p states, lying outside of the coexistence window. Instead of searching for stable oxide TI's with small Δ_i , we attempt to stabilize oxide TI's with large inversion energies.

5. Bringing the topological gene into overlap with the stability gene by applying pressure

Inspired by the fact that many ABO_3 compounds (e.g. BaTiO_3 ^[44]) that are not cubic at ambient conditions can be stabilized under external pressure in the cubic form, we test the

effect of external pressure on the interplay between band inversion and structural stability. We perform similar calculations as Fig. 4(a), but apply external hydrostatic pressure of ≤ 20 GPa. The result of Fig. 4(b) show that the coexistence window for band inversion and structural stability (red background) is significantly extended. At 20 GPa, a stable TI structure can form while tolerating a band inversion of the magnitude of about 2.5 eV. To demonstrate the dramatic effect of pressure on TI-ness versus stability diagram [Fig. 4(b)], we perform enthalpy calculations for BaTeO_3 (from group $\text{II}_A\text{-VI}_B\text{-O}_3$) and RbIO_3 (from group $\text{I}_A\text{-VII}_B\text{-O}_3$). **Figure 5(a,b)** shows the calculated enthalpies of the relevant structure types for BaTeO_3 and RbIO_3 , as a function of hydrostatic pressure, which demonstrate that the cubic perovskite [S1, see red squares in Fig. 5(a,b)] tends to be stabilized by external pressure. At pressure of 15 GPa (35 GPa), the S1 phase that contains the topological gene becomes the lowest-enthalpy structure for BaTeO_3 (RbIO_3). We further check the effect of external pressure on the band inversions in cubic BaTeO_3 and RbIO_3 , finding that the band inversion is not removed by external pressure [see Fig. 5(c,d)], but on the contrary, increased by the pressure from 2.3 eV at 0 GPa to 3.4 eV at 35 GPa for BaTeO_3 , and from 3.0 eV at 0 GPa to 3.8 eV at 35 GPa for RbIO_3 . It is expected because the pressure decreases the atomic bond lengths of BO_6 octahedral, leading to larger s - p repulsion. The enhanced tolerance of cubic ABO_3 structures to band inversions is because of the increased electronic screening effect under pressures. Similar to heavier-chalcogenide TI's (e.g. Bi_2Se_3), the lattice distortions would be screened by the delocalized electronic states. Here, we use external pressure (as an example of external constraints) to tune the screening effect in oxides. Strong screening could exist in oxides without external constraints, such as *covalent oxides* with strong metal-oxygen orbital mixing^[34], pointing to the direction of future search of stable oxide TI's with large inversion energies that is robust under perturbations such as thermal expansion.

6. Conclusions and discussion

Studying the interplay between TI-ness and stability in search of oxide topological insulators opens the door of several scenarios: (i) understanding the general conflicting trends between TI-ness and stability answers the question concerning the rareness of experimentally realizable topological phases, and hopefully discourage false positive predictions of topological insulators in hypothetical, highly unstable structures. (ii) These trends can be readily applied to other band inversion quantum phases, such as topological Dirac semimetals and Weyl semimetals. (iii) The results in this study suggest the directions for future search of stable oxides TI's, that are (a) search for oxides with small inversion energies (b) design large inversion-energy oxide TIs that can be stabilized by external constraints or intrinsic screening effect. This opens the way of rational design of stable oxide TI's using topological genes as pivots, and electronic screening/external constraints (e.g. pressure and strain) as levers.

Methods

DFT total energy and electronic structure evaluation. Total energies were calculated using the projector-augmented wave (PAW) pseudopotential^[37] total energy method without spin-orbit coupling with the exchange-correlation of Perdew-Burke-Ernzerhof (PBE)^[35] as implemented in the Vienna ab-initio simulation package (VASP)^[36]. We use an energy-cutoff of 520 eV and reciprocal space grids with densities of $2\pi \times 0.068 \text{ \AA}^{-1}$ and $2\pi \times 0.051 \text{ \AA}^{-1}$ for relaxation and static calculation, respectively. Electronic structure and physical properties were calculated from DFT taking into account spin-orbit coupling by a perturbation $\sum_{i,l,m} V_i^{SO} \vec{L} \cdot \vec{S} |l,m\rangle_i \langle l,m|$ to the pseudopotential^[45] ($|l,m\rangle_i$ is the angular momentum eigenstate of atomic site i). To illustrate the band inversions, we project the calculated wave function $|\phi\rangle$ on spin and orbital basis of each atomic site $C_{i,l,m,\eta} =$

$\langle \phi | (s_\eta \otimes |l, m\rangle_i \langle l, m|) | \phi \rangle$ and then sum $C_{i,l,m,\eta}$ for a given atomic orbital. The Wigner-Seitz radii for constructing $|l, m\rangle_i$ used in this study are listed in the pseudopotentials of the VASP simulation package^[36]. To illustrate the interplay between band inversion and structural stability, we performed constrained DFT calculations by applying a Hubbard-like external potential term^[43] (V_p) on the I- p orbital in RbIO_3 in the Hamiltonian to gradually remove the band inversion between I- p and I- s states.

Z_2 characterization. For centrosymmetric structures, we evaluate Z_2 from the parities of the wave functions at the time reversal invariant k -points^[39]. For non-centrosymmetric structures, we use the method from Refs.^[38, 46, 47] to calculate the topological invariant Z_2 , which is based on the evolution of Wannier function centers. The topological invariant Z_2 is expressed as the number of times mod 2 of the partner switching between the Wannier function centers during the evolution (as illustrated in Fig. S3). To directly look at the evolution of Wannier function centers, we follow the scheme proposed by Yu *et al.*^[38] The topological nature of a 3D compound is determined by looking at two effective 2D systems with $k_z = 0$ and $k_z = \pi$. Each 2D effective system is then considered as a series of effective 1D system with fixed k_y . For an effective 1D system with periodic condition, the unitary position operator is defined as,

$$\hat{x} = \sum_{j\alpha} e^{-i\delta_{k_x} \cdot \mathbf{R}_j} |j\alpha\rangle \langle j\alpha|, \quad (1)$$

where $\delta_{k_x} = \frac{2\pi}{N_x a_x}$, N_x is the number of real space unit cells along x direction, \mathbf{R}_j denotes the position of the j th lattice site, and α denotes the index of the Wannier function $|j\alpha\rangle$. The projection operator for the occupied subspace for a fixed k_y can be defined as,

$$\hat{P}_{k_y} = \sum_{n \leq 2N, k_x} |\psi_{n\mathbf{k}}\rangle \langle \psi_{n\mathbf{k}}|; \text{ for } k_z = 0 \text{ or } k_z = \pi, \quad (2)$$

where $|\psi_{n\mathbf{k}}\rangle$ is the Bloch state and $2N$ is the number of occupied states.

We then consider the eigenvalue of the projected position operator,

$$\hat{x}_P(k_y) = \hat{P}_{k_y} \hat{x} \hat{P}_{k_y}, \quad (3)$$

that has the following form:

$$\hat{x}_P(k_y) = \begin{bmatrix} 0 & X_{0,1} & 0 & 0 & \cdots & 0 \\ 0 & 0 & X_{1,2} & 0 & \cdots & 0 \\ 0 & 0 & 0 & X_{2,3} & \cdots & 0 \\ \vdots & \vdots & \vdots & \vdots & \vdots & \vdots \\ 0 & 0 & 0 & 0 & \cdots & X_{N_x-2, N_x-1} \\ X_{N_x-1,0} & 0 & 0 & 0 & \cdots & 0 \end{bmatrix}, \quad (4)$$

where $X_{0,1}, X_{1,2}, \dots$ are $2N \times 2N$ matrices. The eigenvalue of the projected position operator can be solved by the transfer matrix method. We define a product of $X_{0,1}, X_{1,2}, \dots$ as,

$$D(k_y) = X_{0,1} X_{1,2} X_{2,3} \cdots X_{N_x-2, N_x-1} X_{N_x-1,0}. \quad (5)$$

$D(k_y)$ has $2N$ eigenvalues:

$$\lambda_m^D(k_y) = |\lambda_m^D(k_y)| e^{i\theta_m^D(k_y)}, m = 1, \dots, 2N. \quad (6)$$

The evolution of the Wannier function center with k_y can be easily obtained by looking at the phase factor θ_m^D (named Wannier center for convenience). The Wannier centers are paired at $k_y = 0$ and $k_y = \pi$, and during the evolution from $k_y = 0$ to $k_y = \pi$, the Wannier center can switch partners, with an odd number of partner switching corresponding to $Z_2 = 1$ (see Supplementary Section II).

Supporting Information

Supporting Information is available from the Wiley Online Library or from the author.

Acknowledgements

Part of the work on calculation of topological properties was supported by NSF Grant titled "Theory-Guided Experimental Search of Designed Topological Insulators and Band-Inverted Insulators" (No. DMREF-1334170). Work on calculation of material stability was supported by Office of Science, Basic Energy Science, MSE division under grant DE-SC0010467 to CU Boulder. This work used the Extreme Science and Engineering Discovery Environment (XSEDE), which is supported by NSF grant number ACI-1053575. We thank Dr. Saicharan Aswartham and Prof. Gang Cao for sharing with us the crystallographic information of the newly synthesized and characterized BaTeO_3 (P2₁/c) structure, and thank Prof. Dan Dessau for helpful discussions.

Received: ((will be filled in by the editorial staff))
Revised: ((will be filled in by the editorial staff))
Published online: ((will be filled in by the editorial staff))

References

- [1] C.L. Kane, E.J. Mele, Z₂ Topological Order and the Quantum Spin Hall Effect, *Phys. Rev. Lett.* **2005**, 95, 146802.
- [2] Z.-C. Gu, X.-G. Wen, Tensor-Entanglement-Filtering Renormalization Approach and Symmetry Protected Topological Order, *Phys. Rev. B* **2009**, 80, 155131.
- [3] B.A. Bernevig, T.L. Hughes, S.-C. Zhang, Quantum Spin Hall Effect and Topological Phase Transition in HgTe Quantum Wells, *Science* **2006**, 314, 1757.
- [4] Y. Cao, J.A. Waugh, X.W. Zhang, J.W. Luo, Q. Wang, T.J. Reber, S.K. Mo, Z. Xu, A. Yang, J. Schneeloch, G.D. Gu, M. Brahlek, N. Bansal, S. Oh, A. Zunger, D.S. Dessau, Mapping the orbital wavefunction of the surface states in three-dimensional topological insulators, *Nat. Phys.* **2013**, 9, 499.
- [5] T.H. Hsieh, H. Lin, J.W. Liu, W.H. Duan, A. Bansil, L. Fu, Topological crystalline insulators in the SnTe material class, *Nat. Commun.* **2012**, 3, 982.
- [6] Z.K. Liu, B. Zhou, Y. Zhang, Z.J. Wang, H.M. Weng, D. Prabhakaran, S.-K. Mo, Z.X. Shen, Z. Fang, X. Dai, Z. Hussain, Y.L. Chen, Discovery of a Three-Dimensional Topological Dirac Semimetal, Na₃Bi, *Science* **2014**, 343, 864.
- [7] X. Deng, K. Haule, G. Kotliar, Plutonium Hexaboride is a Correlated Topological Insulator, *Phys. Rev. Lett.* **2013**, 111, 176404.

- [8] D.J. Kim, J. Xia, Z. Fisk, Topological surface state in the Kondo insulator samarium hexaboride, *Nat. Mater.* **2014**, 13, 466.
- [9] W.A. Harrison, *Electronic Structure and the Properties of Solids: The Physics of the Chemical Bond (Table 7-3)*, Dover Publications, Inc., New York, 1989.
- [10] M.A. Berding, M. van Schilfgaarde, A. Sher, Defect equilibrium in HgTe, *J. Vac. Sci. Technol. B* **1992**, 10, 1471.
- [11] D. West, Y.Y. Sun, H. Wang, J. Bang, S.B. Zhang, Native defects in second-generation topological insulators: Effect of spin-orbit interaction on Bi₂Se₃, *Phys. Rev. B* **2012**, 86, 121201.
- [12] H. Jin, S.H. Rhim, J. Im, A.J. Freeman, Topological Oxide Insulator in Cubic Perovskite Structure, *Sci. Rep.* **2013**, 3, 1651.
- [13] B.H. Yan, M. Jansen, C. Felser, A large-energy-gap oxide topological insulator based on the superconductor BaBiO₃, *Nat. Phys.* **2013**, 9, 709.
- [14] G. Trimarchi, X. Zhang, A.J. Freeman, A. Zunger, Structurally unstable AIIIIBiO₃ perovskites are predicted to be topological insulators but their stable structural forms are trivial band insulators, *Phys. Rev. B* **2014**, 90, 161111.
- [15] G. Li, B.H. Yan, R. Thomale, W. Hanke, Topological nature and the multiple Dirac cones hidden in Bismuth high-T_c superconductors, *Sci. Rep.* **2015**, 5, 10435.
- [16] D. Xiao, W. Zhu, Y. Ran, N. Nagaosa, S. Okamoto, Interface engineering of quantum Hall effects in digital transition metal oxide heterostructures, *Nat. Commun.* **2011**, 2, 596.

- [17] S. Okamoto, W. Zhu, Y. Nomura, R. Arita, D. Xiao, N. Nagaosa, Correlation effects in (111) bilayers of perovskite transition-metal oxides, *Phys. Rev. B* **2014**, 89, 195121.
- [18] Q. Xu, Z. Song, S. Nie, H. Weng, Z. Fang, X. Dai, Two-dimensional oxide topological insulator with iron-pnictide superconductor LiFeAs structure, *Phys. Rev. B* **2015**, 92, 205310.
- [19] J.L.G. Fierro, *Metal Oxides: Chemistry and Applications*, CRC Press, Boca Raton, 2006.
- [20] H. Kawazoe, M. Yasukawa, H. Hyodo, M. Kurita, H. Yanagi, H. Hosono, P-type electrical conduction in transparent thin films of CuAlO₂, *Nature* **1997**, 389, 939.
- [21] R.E. Cohen, Origin of ferroelectricity in perovskite oxides, *Nature* **1992**, 358, 136.
- [22] A. Goldman, *Handbook of Modern Ferromagnetic Materials*, Springer, Boston, 1999.
- [23] J.G. Bednorz, K.A. Müller, Possible high TC superconductivity in the Ba-La-Cu-O system, *Zeitschrift für Physik B* **1986**, 64, 189.
- [24] Y.L. Chen, J.G. Analytis, J.-H. Chu, Z.K. Liu, S.-K. Mo, X.L. Qi, H.J. Zhang, D.H. Lu, X. Dai, Z. Fang, S.C. Zhang, I.R. Fisher, Z. Hussain, Z.-X. Shen, Experimental Realization of a Three-Dimensional Topological Insulator, Bi₂Te₃, *Science* **2009**, 325, 178.
- [25] *Inorganic Crystal Structure Database*, Fachinformationszentrum Karlsruhe, Germany, (2006).

- [26] L.M. Schoop, L. MÜchler, C. Felser, R.J. Cava, Lone Pair Effect, Structural Distortions, and Potential for Superconductivity in Tl Perovskites, *Inorg. Chem.* **2013**, *52*, 5479.
- [27] S.M. Young, S. Zaheer, J.C.Y. Teo, C.L. Kane, E.J. Mele, A.M. Rappe, Dirac Semimetal in Three Dimensions, *Phys. Rev. Lett.* **2012**, *108*, 140405.
- [28] N. Kumada, N. Kinomura, P.M. Woodward, A.W. Sleight, Crystal structure of Bi₂O₄ with beta-Sb₂O₄ -type structure, *Journal of Solid State Chemistry* **1995**, *116*, 281.
- [29] S. Kirklin, J.E. Saal, B. Meredig, A. Thompson, J.W. Doak, M. Aykol, S. Rühl, C. Wolverton, The Open Quantum Materials Database (OQMD): assessing the accuracy of DFT formation energies, *npj Computational Materials* **2015**, *1*, 15010.
- [30] A. Jain, S.P. Ong, G. Hautier, W. Chen, W.D. Richards, S. Dacek, S. Cholia, D. Gunter, D. Skinner, G. Ceder, K.A. Persson, The Materials Project: A materials genome approach to accelerating materials innovation, *APL Materials* **2013**, *1*, 011002.
- [31] S. Terada, H. Tanaka, K. Kubota, Heteroepitaxial growth of Cu₃N thin films, *Journal of Crystal Growth* **1989**, *94*, 567.
- [32] L.G. Wang, A. Zunger, Cluster-Doping Approach for Wide-Gap Semiconductors: The Case of p-Type ZnO, *Phys. Rev. Lett.* **2003**, *90*, 256401.
- [33] D.M. Wood, A. Zunger, Epitaxial effects on coherent phase diagrams of alloys, *Phys. Rev. B* **1989**, *40*, 4062.
- [34] H. Raebiger, S. Lany, A. Zunger, Charge self-regulation upon changing the oxidation state of transition metals in insulators, *Nature* **2008**, *453*, 763.

[35] J.P. Perdew, K. Burke, M. Ernzerhof, Generalized Gradient Approximation Made Simple, Phys. Rev. Lett. **1996**, 77, 3865.

[36] G. Kresse, J. Furthmüller, Efficiency of ab-initio total energy calculations for metals and semiconductors using a plane-wave basis set, Comput. Mater. Sci. **1996**, 6, 15.

[37] G. Kresse, D. Joubert, From ultrasoft pseudopotentials to the projector augmented-wave method, Phys. Rev. B **1999**, 59, 1758.

[38] R. Yu, X.L. Qi, A. Bernevig, Z. Fang, X. Dai, Equivalent expression of Z_2 topological invariant for band insulators using the non-Abelian Berry connection, Phys. Rev. B **2011**, 84, 075119.

[39] L. Fu, C.L. Kane, Topological insulators with inversion symmetry, Phys. Rev. B **2007**, 76, 045302.

[40] C.G. Darwin, The Wave Equations of the Electron, Proceedings of The Royal Society A **1928**, 118, 654.

[41] However, as compared to BaTeO_3 , KIO_3 is a semimetal [see Supplementary Fig. S5] not an insulator, so despite band inversion and well-defined topological invariant Z_2 it is not a topological insulator.

[42] J. Heyd, G.E. Scuseria, M. Ernzerhof, Erratum: “Hybrid functionals based on a screened Coulomb potential” [J. Chem. Phys. 118, 8207 (2003)], J. Chem. Phys. **2006**, 124, 219906.

- [43] S.L. Dudarev, G.A. Botton, S.Y. Savrasov, C.J. Humphreys, A.P. Sutton, Electron-energy-loss spectra and the structural stability of nickel oxide: An LSDA+U study, *Phys. Rev. B* **1998**, 57, 1505.
- [44] T. Ishidate, S. Abe, H. Takahashi, N. Môri, Phase Diagram of BaTiO₃, *Phys. Rev. Lett.* **1997**, 78, 2397.
- [45] P. Błoński, J. Hafner, Magnetic anisotropy of transition-metal dimers: Density functional calculations, *Phys. Rev. B* **2009**, 79, 224418.
- [46] L. Fu, C.L. Kane, Time reversal polarization and a Z₂ adiabatic spin pump, *Phys. Rev. B* **2006**, 74, 195312.
- [47] A.A. Soluyanov, D. Vanderbilt, Computing topological invariants without inversion symmetry, *Phys. Rev. B* **2011**, 83, 235401.

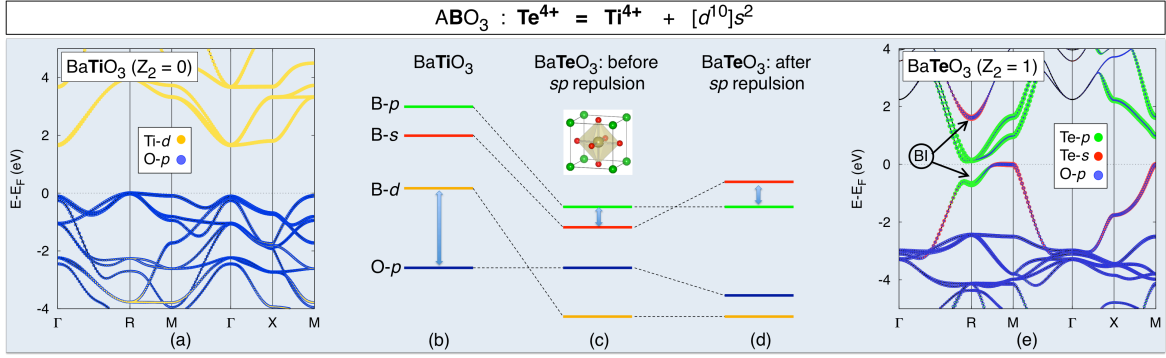


FIG. 1. Illustration of the topological gene in cubic ABO_3 by electronic structures in DFT of $BaTiO_3$ (a) and $BaTeO_3$ (e) with cubic perovskite ($Pm-3m$) structure (at zero pressure), and schematic orbital diagram of ABO_3 perovskite compounds, in the cases of (b) electron-poor B atom such as Ti in $BaTiO_3$ where there is no band inversion, (c) and (d) electron-rich (“lone pair”) B atom such as Te having additional $d^{10}s^2$ orbital shells, leading to band inversion in $BaTeO_3$. The vertical blue arrows indicate the fundamental band gaps. The inset in (c) shows the “topological gene”—associated with topological insulation in this class of compounds. BI denotes band inversion with arrows pointing to the inverted states. The dotted lines with different colors denote the band projection onto different atomic orbitals.

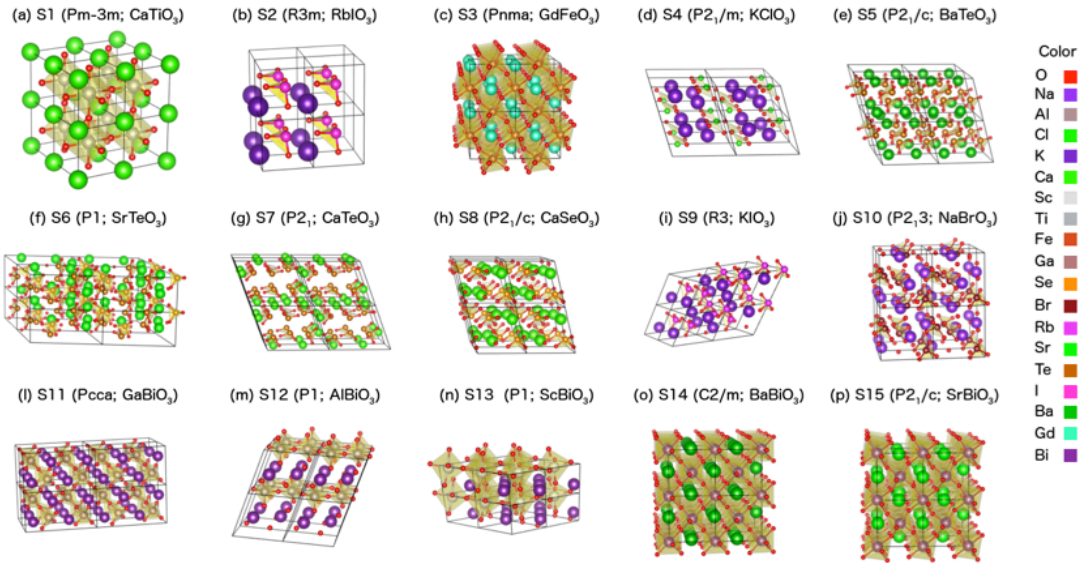


FIG. 2. Illustration of the geometry of the structures of ABO₃ discussed (a-p). The legend of coloring for distinguishing atoms of different chemical elements is displayed on the right. The black boxes in each structure represent the unit cell, and 2×2×2 supercells were shown for better visual understanding. All triangle or tetragonal yellow structure corresponds to bonding from elements to oxygen with a distance lower than 2.4 Å.

| VI_B II_A | Te | Se | VI_B I_A | I | Br | A G. | Ga/Y/Ba | Al/Sc/Sr |
|--------------------------------|--|--|-------------------------------|---|--|------------------|---|---|
| Ba | BaTeO ₃ S1 (156) : R ¹ S2 (76) : NI S3 (37) : NI S4 (3) : NI S5 (0) : NI | BaSeO ₃ S1 (366) : R ¹ S2 (75) : NI S3 (63) : NI S4 (0) : NI | Rb | RbIO ₃ S1 (241) : R ¹ S3 (37) : NI S4 (24) : NI S2 (0) : NI | RbBrO ₃ S1 (551) : R ¹ S3 (20) : NI S4 (5) : NI S2 (0) : NI | III _B | <i>GaBiO₃</i> S1 (223) : NI S2 (76) : NI S3 (71) : NI S4 (48) : NI S11 (0) : NI | <i>AlBiO₃</i> S1 (97) : NI S4 (81) : NI S3 (44) : NI S2 (38) : NI S12 (0) : NI |
| Sr | SrTeO ₃ S1 (232) : R ¹ S2 (43) : NI S4 (14) : NI S6 (9) : NI S3 (0) : NI | SrSeO ₃ S1 (353) : R ¹ S2 (68) : NI S3 (25) : NI S4 (0) : NI | K | KIO ₃ S1 (190) : R ¹ S3 (22) : NI S4 (21) : NI S2 (6) : NI S9 (0) : NI | KBrO ₃ S1 (476) : R ¹ S3 (9) : NI S2 (3) : NI S4 (0) : NI | III _A | <i>YBiO₃</i> S1 (629) : NI S4 (39) : NI S2 (31) : NI S3 (0) : NI | <i>ScBiO₃</i> S1 (325) : NI S4 (77) : NI S2 (27) : NI S3 (10) : NI S13 (0) : NI |
| Ca | CaTeO ₃ S1 (426) : R ¹ S4 (76) : NI S2 (52) : NI S3 (17) : NI S7 (0) : NI | CaSeO ₃ S1 (449) : R ¹ S2 (46) : NI S4 (46) : NI S3 (12) : NI S8 (0) : NI | Na | NaIO ₃ S1 (224) : R ¹ S2 (56) : NI S4 (34) : NI S3 (0) : NI | NaBrO ₃ S1 (469) : R ¹ S2 (51) : NI S4 (36) : NI S3 (7) : NI S10 (0) : NI | II _A | <i>BaBiO₃</i> S4 (76) : NI S1(23) : R ¹ e S3 (4) : NI S14 (0) : NI | <i>SrBiO₃</i> S1(142):R ¹ e S2 (119) : NI S4 (69) : NI S3 (14) : NI S15 (0) : NI |

FIG. 3. Presence of topological properties (indicated by red, with R¹ denoting the single band inversion at R point in BZ) vs absence (indicated by black, with NI denoting normal insulator) and relative DFT total energies (meV/atom, with zero indicating the ground state, shown in parentheses) of ABO₃ compounds with different crystal structures S1-S15 (see Fig. 2) at zero pressure. The calculations included swapping of A and B elements on the ABO₃ atomic sites and the lower-energy configuration is selected. All considered compounds except YBiO₃, ScBiO₃, GaBiO₃ and AlBiO₃ (shown in italics; note that in their lower-energy S1 structure, Bi is at the A site), are thermodynamically stable in their lowest-energy structure, as found by DFT calculations of the convex hull [29, 30]. For BaBiO₃, the initial S2 structure relaxes into the S1 structure, thus the total energy of S1 but not S2 structure is reported. For BaBiO₃ (as well as SrBiO₃) in the S1 structure, the band inversion (denoted as R¹e) occurs only after doping by 1 electron/formula unit (see Supplementary Fig. S1), but not at the band edges as for the other cases.

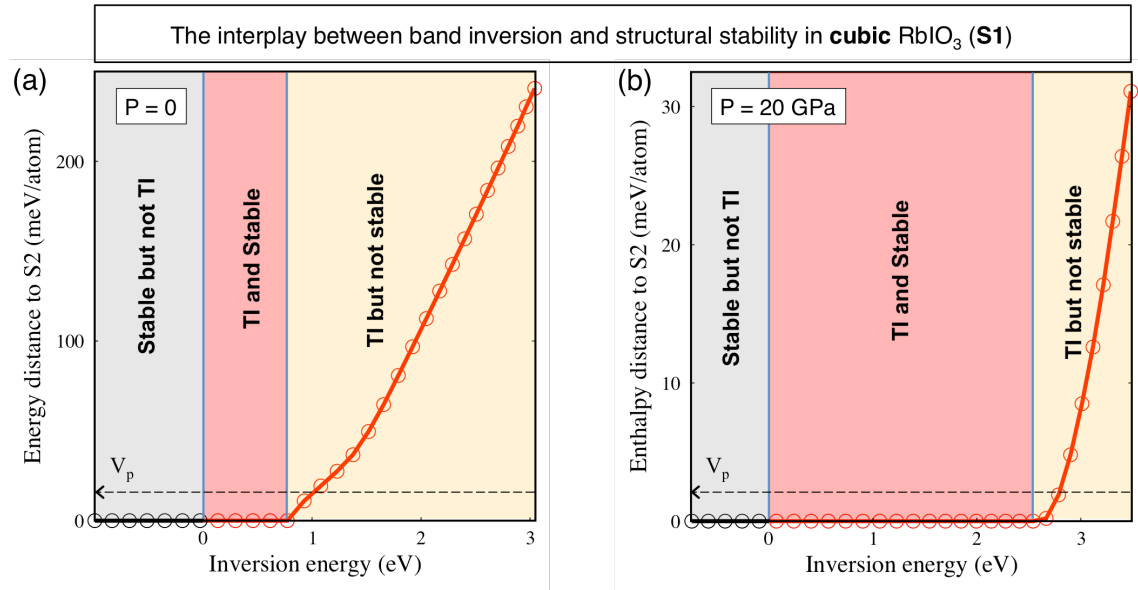


FIG. 4. Illustration of the interplay between band inversion and structural stability in cubic RbIO₃ at 0 GPa (a) and 20 GPa (b). The inversion energy in the cubic system is tuned by applying an external potential (V_p ; $V_p = 0$ corresponds to the largest inversion energy) [see the evolution of electronic structures with decreasing inversion energy for 0 GPa and 20 GPa in Supplementary Fig. S8 and Fig. S9, respectively].

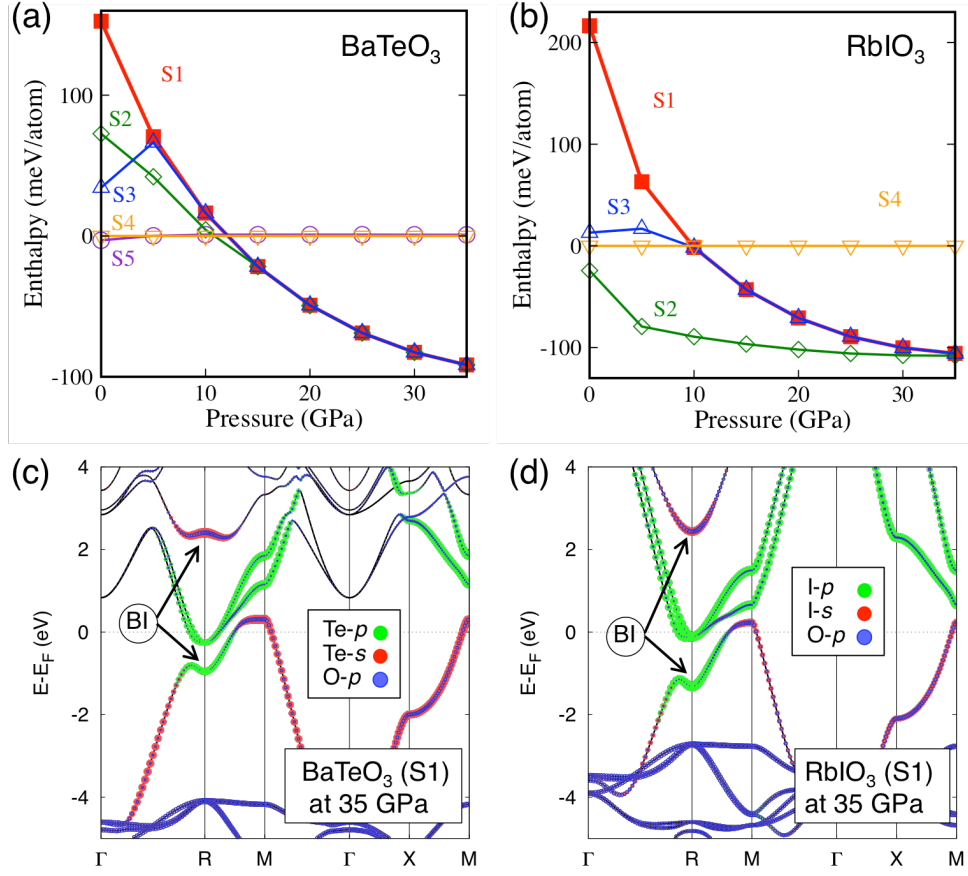


FIG. 5. Enthalpies of (a) BaTeO₃ and (b) RbIO₃ in the ABO₃ structures as functions of pressure, illustrating that the cubic perovskite structure (S1) with the topological gene becomes the lowest-enthalpy structure at moderately high pressure. For graphic clarity, the enthalpies of the S4 structures (P2₁/m) are chosen as the zero at each pressure. Swapping of A and B sites has been considered, and the lowest-energy configuration is selected. (c-d) Electronic structures of cubic BaTeO₃ (c) and RbIO₃ (d) under external pressure of 35 GPa. The band inversion is denoted in the figure by BI, with arrows pointing to the inverted states. The dotted lines with different colors denote the band projection onto different atomic orbitals.